41st AIAA Fluid Dynamics Conference and Exhibit
27 - 30 June 2011, Honolulu, Hawaii

AIAA 2011-3990

Numerical Investigation of Serpentine Plasma Actuators for Separation Control at Low Reynolds Number

Mark Riherd[1] and Subrata Roy[2]
Applied Physics Research Group, Department of Mechanical and Aerospace Engineering, University of Florida, Gainesville, FL 32054

Miguel Visbal[3]
Computational Sciences Branch, Air Vehicle Directorate, Air Force Research Laboratory, WPAFB, OH 45433

Dielectric Barrier Discharge (DBD) plasma actuators with serpentine shaped electrodes cause a change in the operational behavior of the flow control mechanism relative to the standard 'linear' actuator due to the introduction of fully three dimensional vortices. A parametric study is performed on a partially separated transitional flow over an SD7003 airfoil. This study examines the change in behavior as a function of geometric parameters, in particular the geometric amplitude of the serpentine geometry as it is flattened out, reverting back to the standard linear actuator. Continuous operation of the actuator does not fully remove the separation, but it does modify the properties of the separated boundary layer. Separation is eliminated when the actuator is operated with a duty cycle.

Nomenclature

c	=	Chord length
C_D	=	Coefficient of drag
C_f	=	Coefficient of skin friction
C_L	=	Coefficient of lift
C_M	=	Coefficient of moment
C_p	=	Coefficient of pressure
D_c	=	Nondimensional plasma force magnitude
E	=	Energy
E_0	=	Characteristic electrical field
e_c	=	Electron charge
ξ, ζ, η	=	Body fitted coordinates
f_i	=	Body force in the i direction
St	=	Nondimensional forcing
F, **G**, **H**	=	Inviscid flux vectors
$\mathbf{F_v}$, $\mathbf{G_v}$, $\mathbf{H_v}$	=	Viscid flux vectors
γ	=	Ratio of specific heats
$\mathcal{J}$	=	Jacobian
M	=	Mach number
p	=	Pressure
ρ	=	Density
ρ_c	=	Characteristic electron density
Q_i	=	Heat Flux
Q	=	Vector of dependent flow variables
U, V, W	=	Contravariant velocity components
u, v, w	=	Velocity in the Cartesian coordinate system

[1] Graduate Research Assistant, AIAA Student Member
[2] Associate Professor, AIAA Associate Fellow
[3] Technical Area Leader, Computational Sciences Branch, AFLR/RBAC, AIAA Associate Fellow

Re	=	Reynolds number
$\boldsymbol{S}$	=	Source term vector
St	=	Strouhal number
τ	=	Nondimensional time
τ_{ij}	=	Shear stress
x,y, z	=	Cartesian coordinates

Subscripts

∞	=	Freestream reference velocity
xi	=	Partial derivatives with respect to the x_i^{th} direction

I. Introduction

Separated flows and the methods used to reattach them are two highly documented issues in flow control research[1]. The separated flows that can exist over airfoils have a number of performance reducing properties, including increased drag, stronger vortex shedding and reduced ratio of lift to drag, among other effects. Reattachment of these flows at low Reynolds number is of vital importance to many Micro Air Vehicle (MAV) applications. For these types of applications, the flow often has some level of laminar behavior, which is important for control of the flow, as transitioning these flows can lead to reattachment.

DBD plasma actuators have a number of beneficial properties that are unseen in other flow control devices[2-4]. The devices themselves have no moving parts, and respond on the time scale of an electrical device, far faster than the fluid itself. Plasma actuators can also be flush mounted such that they have no impact on the flow field when not in use. Furthermore, DBD plasma actuators have shown themselves to be effective for boundary layer control[4-6] and for flow reattachment at low Reynolds number[6-11], especially when used in a pulsed manner, where unstable frequencies can be excited, causing the flow to transition and then reattach.

Plasma actuators with novel geometries, such as the serpentine geometry have shown themselves to be very useful in a number of numerical studies[11-14] as well as limited experimental work[15-17]. These actuators are able to introduce streamwise, as well as spanwise and surface normal vorticity to the flow, and promote increased mixing of the flow.

This study aims to generalize the geometry of the plasma actuator electrodes and explore the flow physics as this geometry is modified. In this generalization, the standard actuator is considered to be a special case of the serpentine geometry (with infinite wavelength and zero amplitude) where no streamwise or surface normal vorticity is added to the flow by the actuator except for at the spanwise edges of the electrodes. While published results show an interesting difference in the physics when the electrode geometries are distinctly different[10], the numerical simulations performed for this work hope to fill the knowledge gap as the actuator is smoothly transitioned from the serpentine geometry to the linear geometry.

II. Serpentine Geometry Plasma Actuation

DBD plasma actuators are small, electrically powered devices composed of two asymmetrically placed electrodes, one exposed and one encapsulated in a dielectric material. A high electrical potential is applied between the two electrodes. The electrical field in this region causes gas on the surface near the two electrodes to become weakly ionized[2]. The ions and electrons in the flow are imparted momentum via the electric field, and through collisional processes, momentum is imparted to the remaining neutral fluid particles.

Novel plasma actuator geometries, such as the finger geometry of Satchzman et al.[15] or the plasma synthetic jets developed by Santhanakrishnan and Jacob[16] have been used for various flow control applications. The serpentine plasma actuator developed by Roy and Wang[12-14] has its own benefits in that

it is able to induce spanwise and streamwise vorticity (through the $\nabla \times \vec{f}_b$ term in the vorticity equation), while still maintaining relatively simple electrode geometry that can be extended indefinitely to any distance (Figure 1). This geometry is also significant in that it is able to define a characteristic spanwise wave length to the flow control, which is important with respect to exciting certain unstable modes in order to transition the flow.

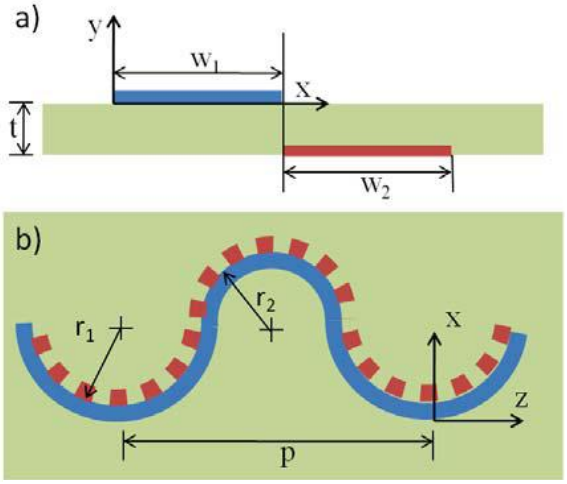

Figure 1. Serpentine geometry from the side (a) and from above (b). From Durscher and Roy, 2011, used with permission.

III. Governing Equations and Numerical Models

This study was performed using the Implicit Large Eddy Simulation (ILES) method[18,19] using the implicit Beam and Warming algorithm[20] for time integration. The unsteady, three dimensional, compressible, unfiltered form of the Navier-Stokes equations is solved, and then a Pade type filter such as those developed by Lele[21] is applied. The equations are solved in a generalized body-fitted coordinate system. The equations are solved in the conservation form, where

$$\frac{\partial}{\partial t}\left(\frac{1}{\mathcal{J}}\mathbf{Q}\right)+\frac{\partial}{\partial \xi}\left(\boldsymbol{F}-\frac{1}{Re}\boldsymbol{F_v}\right)+\frac{\partial}{\partial \eta}\left(\boldsymbol{G}-\frac{1}{Re}\boldsymbol{G_v}\right)+\frac{\partial}{\partial \zeta}\left(\boldsymbol{H}-\frac{1}{Re}\boldsymbol{H}\right)=D_c q_c \boldsymbol{S}$$

Q is the vector of dependent variables. The terms F, G, and H are the inviscid flux vectors, and F_v, G_v, and H_v are the viscid flux vectors. Furthermore t represents time, and ξ, η, and ζ represents the body fitted coordinate system. The plasma forcing is included via the source term S, explained in more depth below. While this is an incompressible flow, because a compressible flow solver is used, a Mach number of 0.1 is used in order to minimize compressibility effects while maintaining numerical stability. There terms are defined as the dependent variables as

$$\boldsymbol{Q}=\begin{bmatrix}\rho\\ \rho u_1\\ \rho u_2\\ \rho u_3\\ \rho E\end{bmatrix},$$

the inviscid flux vectors are

$$\boldsymbol{F}=\frac{1}{\mathcal{J}}\begin{bmatrix}\rho U\\ \rho u_1 U+\xi_1 p\\ \rho u_2 U+\xi_2 p\\ \rho u_3 U+\xi_3 p\\ \rho E U+\xi_i u_i p\end{bmatrix},\qquad \boldsymbol{G}=\frac{1}{\mathcal{J}}\begin{bmatrix}\rho V\\ \rho u_1 V+\eta_1 p\\ \rho u_2 V+\eta_2 p\\ \rho u_3 V+\eta_3 p\\ \rho E V+\eta_i u_i p\end{bmatrix},\quad \text{and}\quad \boldsymbol{H}=\frac{1}{\mathcal{J}}\begin{bmatrix}\rho W\\ \rho u_1 W+\zeta_1 p\\ \rho u_2 W+\zeta_2 p\\ \rho u_3 W+\zeta_3 p\\ \rho E W+\zeta_i u_i p\end{bmatrix},$$

the viscid flux vectors are

$$\boldsymbol{F_v}=\frac{1}{\mathcal{J}}\begin{bmatrix}0\\ \xi_{x_i}\tau_{i1}\\ \xi_{x_i}\tau_{i2}\\ \xi_{x_i}\tau_{i3}\\ \xi_{x_i}(u_j\tau_{ij}-\mathcal{Q}_i)\end{bmatrix},\qquad \boldsymbol{G_v}=\frac{1}{\mathcal{J}}\begin{bmatrix}0\\ \eta_{x_i}\tau_{i1}\\ \eta_{x_i}\tau_{i2}\\ \eta_{x_i}\tau_{i3}\\ \eta_{x_i}(u_j\tau_{ij}-\mathcal{Q}_i)\end{bmatrix},\qquad \text{and}\qquad \boldsymbol{H_v}=\frac{1}{\mathcal{J}}\begin{bmatrix}0\\ \zeta_{x_i}\tau_{i1}\\ \zeta_{x_i}\tau_{i2}\\ \zeta_{x_i}\tau_{i3}\\ \zeta_{x_i}(u_j\tau_{ij}-\mathcal{Q}_i)\end{bmatrix}$$

where

$$U=\xi_{x_i}u_i\,,\qquad V=\eta_{x_i}u_i,\qquad \text{and}\qquad W=\zeta_{x_i}u_i$$
$$E=\frac{T}{\gamma(\gamma-1)M_\infty^2}+\frac{1}{2}(u^2+v^2+w^2)$$

p represent the pressure. ρ represents density. T represents temperature, and finally, E represents energy. All of these variables have been nondimensionalized by their characteristic values, except for pressure, which has been nondimensionalized by the dynamic head of the characteristic variables. The length scales have all been nondimensionalized by the chord length of the airfoil.

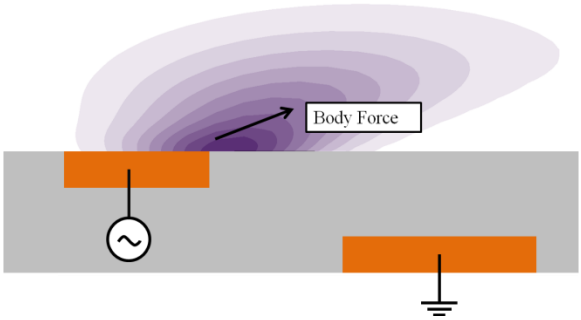

Figure 2. Schematic of a DBD plasma actuator and the model of the body force.

The plasma body force comes from the Townsend ionization of the air between two asymmetrically placed electrodes, separated by a dielectric material (Figure 2). The magnitude of this forcing is controlled by the nondimensional parameter D_c, being the ratio of twice the maximum possible plasma work to the dynamic head as shown below. A reduced order model[22] for the plasma was used. While this model is simplest of the available models, the primary purpose of the plasma in these simulations is not an in depth study of the plasma kinetics, but how disturbances due to plasma actuation affects the flow overall. Additionally, recent results[10] have shown that there is relative independence of the plasma model to the end result under certain conditions, similar to what is used in this simulation in this simulation. The plasma source is formally described for these simulations as

$$\boldsymbol{S}=\frac{1}{\mathcal{J}}\begin{bmatrix}0\\ f_x\\ f_y\\ f_z\\ f_iu_i\end{bmatrix}\text{ and }D_c=\frac{\rho_{e^-}e_cE_0c}{\rho_\infty u_\infty^2}$$

The computations for this study were done on a cylindrical O-mesh of 390x242x97 (angular x radial x spanwise) points representing an SD7003 airfoil with a unit chord length and extended 0.2 chord lengths in the spanwise direction. The mesh extends radially outwards 100 chord lengths in order to provide a good free stream condition. The mesh is also stretched as it goes to the free stream in order to prevent reflections off of the free stream boundary. Periodic boundary conditions were applied in the spanwise and angular directions. The baseline flow case was also on a comparable mesh with 650x390x151 points representing the same domain in order to check for grid independence of the solution.

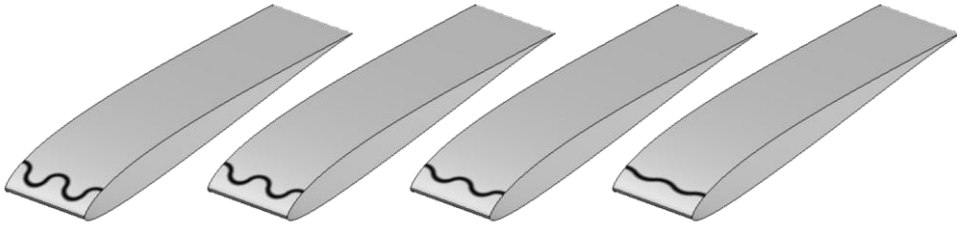

Figure 3. Geometries of the serpentine force distributions. From left to right - Full, three quarters, half, and quarter amplitudes of the serpentine geometry.

Force Geometry	Amplitude (r)	Wavelength (p)
Full	0.02500	0.1
Three quarters	0.01875	0.1
Half	0.01250	0.1
Quarter	0.00625	0.1

Table 1. Details of the plasma actuator geometries.

Case	Force Geometry	Pulsing Freq. (St)	D_c
Baseline	None	n/a	n/a
Baseline – fine	None	n/a	n/a
Full – Continuous	Full	5.0	3.27
Three quarters – Continuous	Three quarters	5.0	3.27
Half – Continuous	Half	5.0	3.27
Quarter – Continuous	Quarter	5.0	3.27
Full – Pulsed	Full	n/a	3.27
Three quarters – Pulsed	Three quarters	n/a	3.27
Half – Pulsed	Half	n/a	3.27
Quarter – Pulsed	Quarter	n/a	3.27

Table 2. Description of the plasma body force for the cases run

A baseline flow for the SD7003 airfoil was established after running for 100,000 (10 non-dimensional units of time, τ, where $\tau=u_\infty/c$) times steps ($\Delta\tau=0.0001$) to remove any transient irregularities. This flow was used as an initial condition for all of the cases tested. All of the cases were run for at least 5τ in order to reach an equilibrium state where the transient effects could be considered negligible. Statistics were then collected over a period of $3.2\ \tau$ (equivalent to 16 cycles of plasma forcing).

IV. Results and Discussion

A. Baseline Case

A baseline case was run in order to establish a control case from which the others can be compared to. The solution to flow over an SD7003 airfoil at a Reynolds number of 40,000 with a 4º angle of attack shows a separated shear layer over the upper surface of the airfoil. This shear layer is laminar in nature, but roughly two thirds down the chord length the flow transitions and reattaches to the surface of the airfoil. The flow over the last two thirds of the airfoil continues to transition, and once the flow reaches the trailing edge of the airfoil, it is fully turbulent (Figure 4a).

A region of low momentum exists in the separation bubble. This bubble is largely steady in nature, except for near the transition point (Figure 4b). This bubble is largely steady in nature, except for near the transition point (Figure 4b).

This flow also shows a quasi-periodic shedding of vortical structures starting within the laminar shear layer with a frequency around St=5, indicating that some sort of instability exists near that frequency. Previous[10,11] have taken advantage of this instability to remove the flow separation and those studies were able to produce an attached flow.

In addition to the structure of the flow, the size and shape of the separation bubble match sufficiently well with previously reported experimental and numerical data[23-25].

B. Continual actuation with serpentine geometry – flow and surface features

Running the serpentine geometry with continuous actuation allows for continual streamwise vorticity to be added to the flow as a function of the geometry, isolating the effects of streamwise vorticity insertion from those of any pulsed flow stability, which are addressed below in Sec. 4C.

As the amplitude of the serpentine geometry and the amount of streamwise vorticity is increased, the separated shear layer begins to show waviness to it, as the streamwise vorticity lifts it in certain areas, and depresses it in others (Figure 5). This waviness shows that the actuator is having an effect on the boundary layer, even though the separated region is not attaching.

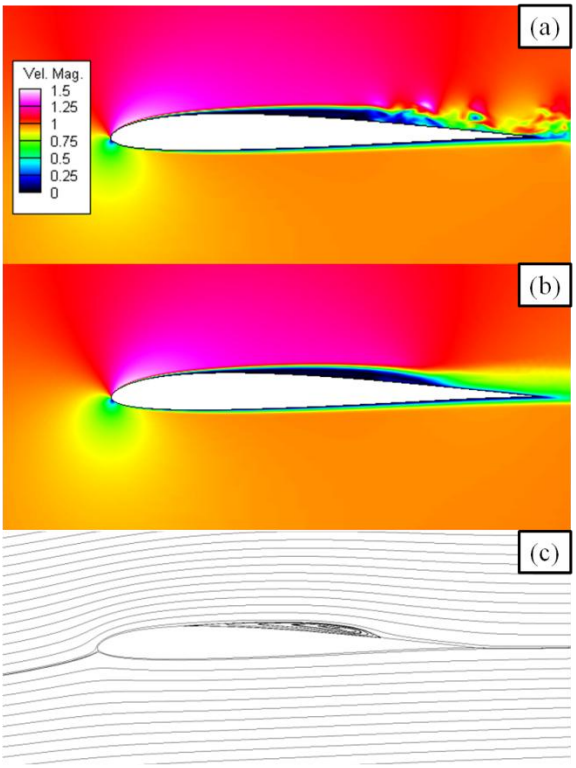

Figure 4. Instantaneous velocity magnitude (a), time and spanwise averaged velocity magnitude (b), and streamlines of the time and spanwise averaged flow (c).

Previous studies[10] have shown this type of continuous serpentine actuation to be effective for separation control using more concentrated plasma forcing (over a smaller volume, but with the same total amount of force). However, in the present study, the shear layer does not break down, and separation control is not achieved. Because the forcing here is less compact than the forcing used in that study, a significant portion of it is inserted outside of the boundary layer. As much of the force is inserted outside the boundary layer, less of the total force is available to perturb the boundary layer itself and is used to perturb the free stream, which has a lesser effect on the flow, though enough of the body force is still present in order to perturb the flow.

The time averaged flow field confirms that the flow is still separated, and further shows that the transitional effects are not strongly impacted (Figure 6). Additionally, the primary effect seems to be slight forward movement of the transition of the shear layer as the geometry of the serpentine actuator becomes more pronounced. Even still, the thickness of the wake and the velocity deficit seem to be nearly constant. The lack of streamwise vortical effects via the Q-criterion[26] indicates that the actuator is not causing streamwise rotational effects. Instead, it is introducing more shear stress than rotational stress in the streamwise direction.

The time averaged surface pressure shows that a plateau of surface pressure exists for the uncontrolled case. This is typical of recirculating, separated flows. As the continuous plasma flow control is applied, the shape of this plateau changes, shortening in length, but slightly increasing in height as the serpentine geometry becomes fuller (Figure 7a). This change in the surface pressure profile suggests that the laminar boundary layer is thickening (causing a larger pressure drop), but transitioning slightly quicker.

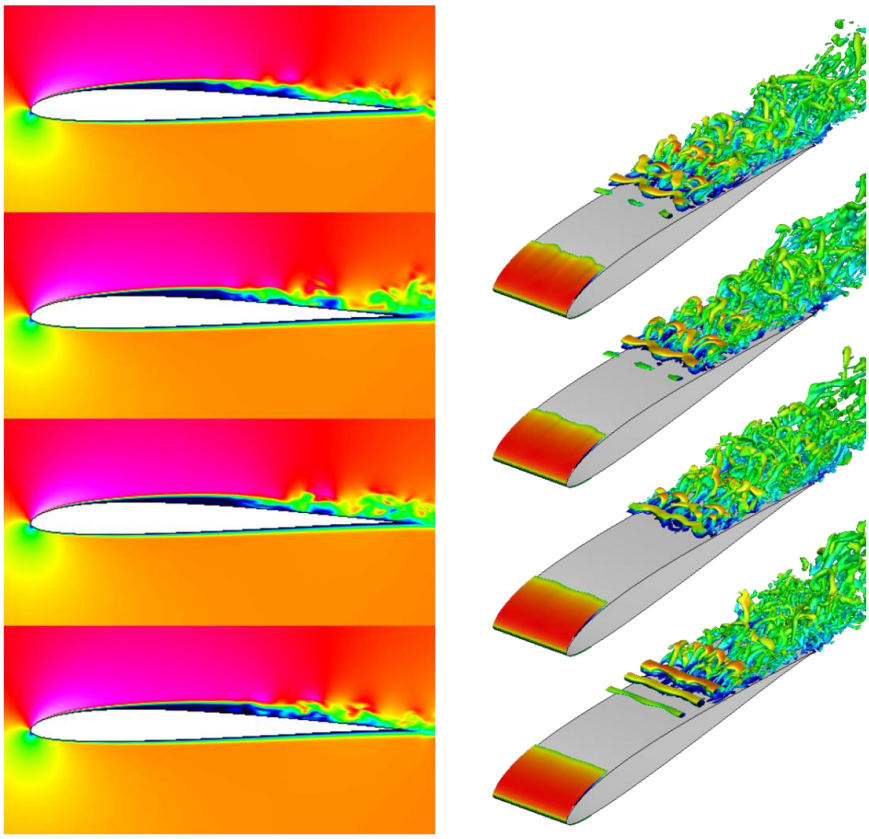

Figure 5. Velocity magnitude (at z=0.1 the pinching point, left) and Q-criterion (Q=100, right) for the cases of continual serpentine plasma actuation, varying the geometry of the actuator (from top to bottom - full, three quarters, half and one quarter).

Subtracting the spanwise average from the time averaged of the surface pressure coefficient, one can see that there is a certain noisy periodicity to the surface pressure with the roughly the same spanwise wave number as that of the plasma actuator even after 100 samples (Figure 7b-e). This is another indicator that while the separation is not removed using continual actuation, there are subtle effects of the actuation on the flow. Using a stronger actuator would amplify these effects, and eventually control could be achieved using could eventually be achieved using continuous actuation.

The power spectral density (Figure 8) shows that not much changes significantly as the continuous plasma control is applied. The growth of the turbulent kinetic energy (Figure 9) shows that there is upstream movement of the unsteady effects in the laminar shear layer that ultimately lead to the flow transitioning and reattaching as the geometry of the plasma actuation is increased. However, the primary growth rate of this turbulent kinetic energy remains constant for all of the cases, including the case of no plasma actuation.

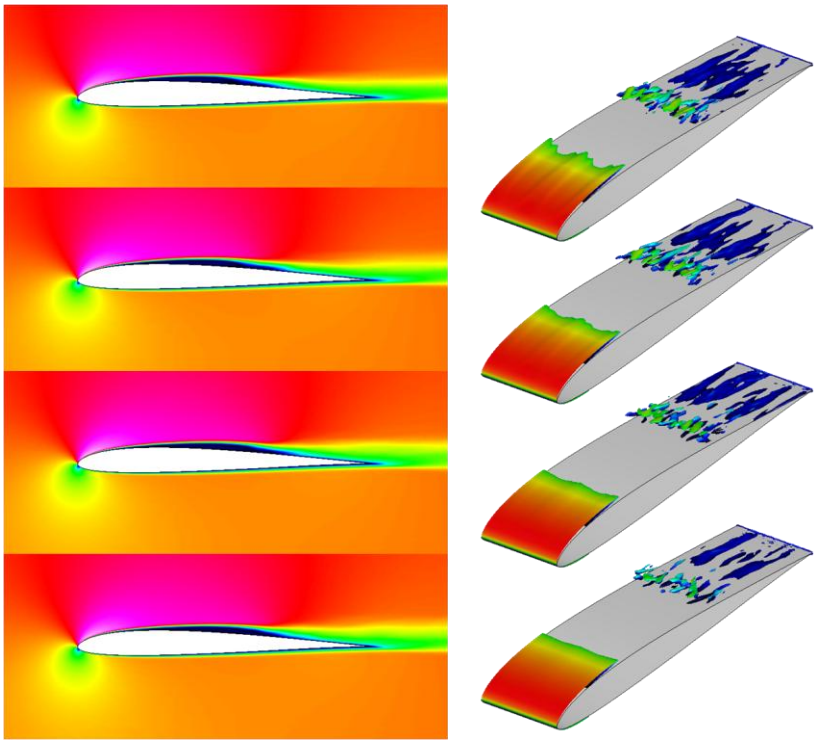

Figure 6. Time averaged velocity magnitude (z=0.1, pinching point, left) and Q-criterion (Q=100, right) for the cases of continual serpentine plasma actuation, varying the geometry of the actuator (from top to bottom – full, three quarters, half and one quarter).

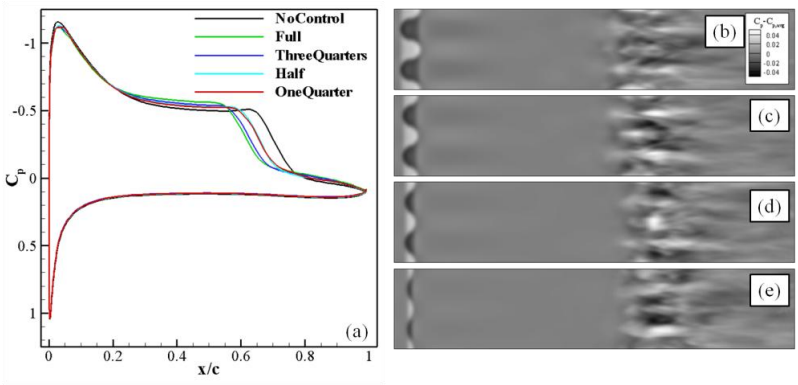

Figure 7. Time and spanwise averaged coefficient of pressure, C_p, on the surface of the airfoil (a) and time averaged local variations in the surface pressure coefficient - $C_p(x,z)-C_{p,avg}$ From top to bottom – Full, three quarters, half and one quarter (b-e).

C. Pulsed actuation with the serpentine geometry – flow and surface features

While the steady actuation shows limited degrees of success, when the actuation is pulsed at a frequency corresponding to instabilities in the shear layer, the reattachment is much more successful. The pulsed actuation causes the shear layer to transition and reattach. The boundary layer stays attached over the airfoil surface, the wake thins, and the drag experienced by the airfoil drops.

The transitional vortical structures produced by the plasma actuation seem to be regular in structure These structures consist of a large hairpin structure and a more mobile smaller, hairpin structure component (Figures 10, 11). The large component is aligned with the spreading portion of the actuator geometry in the streamwise direction, while the smaller structure is aligned with the pinching portion of the actuator and lags behind the larger structure due to lower velocities closer to the airfoil surface.

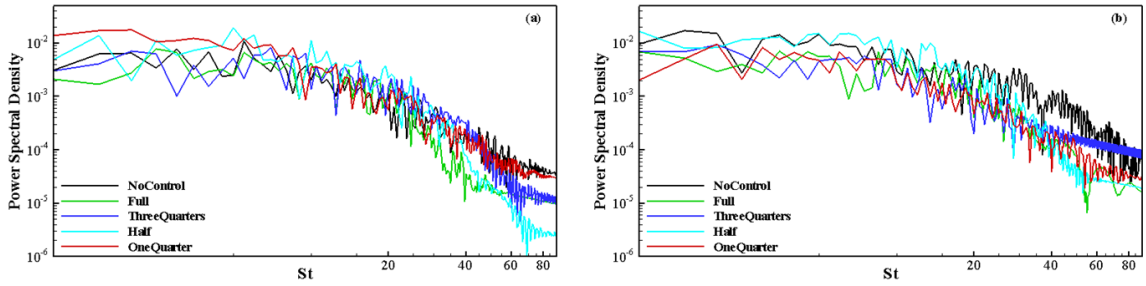

Figure 8. Power spectral density for the continuous actuation for x/c=0.5 (a) and 0.9 (b).

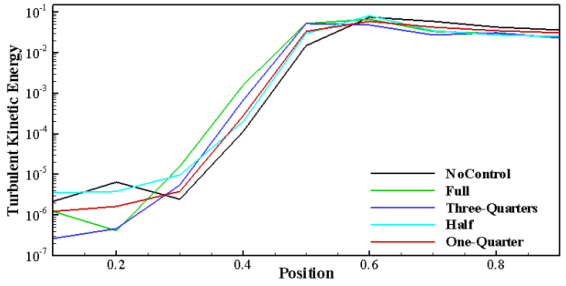

Figure 9. Growth of turbulent kinetic energy along the surface of the airfoil with continuous actuation.

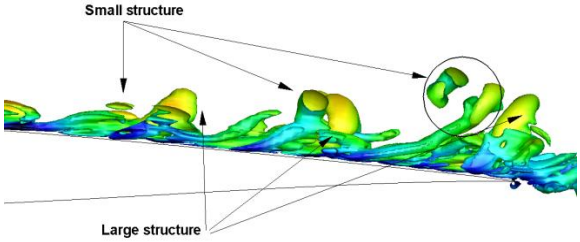

Figure 10. Side view of the vortical structures from the pulsed actuation near the trailing edge.

These structures arise due to instabilities in the shear layer as it extends over the surface in the non-actuated portion of the duty cycle during the no plasma portion of the duty cycle. When they are initially formed, the larger structure (formed in the spreading region of the actuation) is very wide, and extends upwards to the surface of the boundary layer, while the smaller structure (formed in the region of the pinching actuation) is more compact and resides in the lower portion of the boundary layer. As these move downstream, the smaller structure is thrust upwards because of the small amount of streamwise vorticity generated by the plasma actuator. This upward motion continues for the smaller vortex, which continues to grow as it convects downstream. As the two vortical structures pass over the trailing edge of the airfoil, the smaller structure has reached a similar height as the large vortical structure, if not reaching above it.

It should be noted that while only the largest scale structures are easily visible for (Q=100), these structures are not single hairpin vortices, but packets of them, with additional hairpin vortices propagating off of the larger, initial structure as the packet moves downstream in a manner consistent with that of hairpin structures on a flat plate[27-30]. For higher grid resolutions, the finer and finer structure associated with the vortices would become more visible and better resolved.

From the comparison of the phase averaged and instantaneous flow, it can be seen that the two are very similar (Figure 13). The only noticeable difference is that the smallest unsteady structures have averaged out, most noticeable near the trailing edge and the wake. This suggests that the structures and their mixing are largely deterministic, and caused by the interaction of the shear layer and the plasma actuation. However, as these effects convect downstream, they transition into successively smaller and more random components.

The phased averaged flow at the tail still exhibits very complex, yet seemingly periodic behavior (Figure 14). This indicated that a majority of the structures over the airfoil are deterministic in nature, and are repeated ever cycle. However, in the wake, it seems that there are more randomized components to the flow, and these components average out over a given number of samples.

At the larger scale, these structures are periodic in the spanwise direction. This is due to the dictation of a dominant spanwise wave length by the serpentine plasma actuator. If this wavelength were varied, the length scale of the periodic behavior would change to match it.

For the time averaged data, it can be seen that the flow does ultimately reattach, and in examining the Q-criterion, that some streamwise structures are created. These spanwise variations would not be present for a standard linear configuration (Figure 15, right). The large structures seen in the flow eventually average out, which exposes the underlying streamwise vorticity added by the plasma actuators (though some of this may be due to the regularity and length of the hairpin vortex legs). While the pattern of streamwise vorticies seen here seems very complicated, it should be recognized that the streamwise vortices farther in the leading portion of the chord leads to the hairpin vortical structures that later dominate the flow. Additionally, since the vortical structures aren't directly connected to the actuator, the streamwise oriented structures are most likely a by-product of the actuation, a remnant of the disturbances introduced, not a direct contribution by the serpentine flow control. This does not mean that there is negligible addition of streamwise vorticity. The Q-criterion locates vortical structures based on the dominance of rotational stresses over irrotational stresses, not only the presence of streamwise vorticity, therefore, just as with the continual actuation, more shear than rotation is being added to the flow.

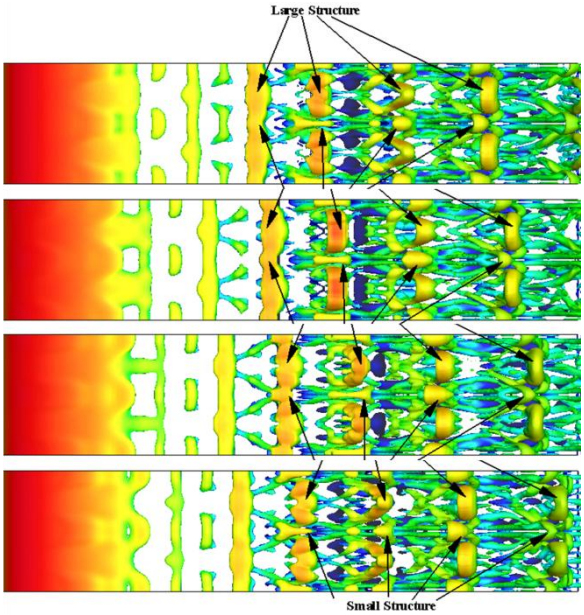

Figure 11. Interaction of the hairpin vortices from the phase averaged case with the full electrode geometry during a complete cycle of plasma actuation in increments of $\pi/2$ starting from the top. The Q-criterion (Q=100) is shown, colored by the velocity magnitude.

The time averaged data also shows that there are slight regions of low momentum fluid over the surface of the airfoil (Figure 15, left). While these might be considered to be problematic, increasing the strength of the plasma actuator (either by additional force, or a denser, more compact force) would easily solve this.

There also appear to be variations in the wake that vary with respect to the geometry of the plasma actuation. These variations are due to the size and shape of the hairpin vortices that are created. Two effects are occurring as the geometry of the device is changed.

Examining the power spectral density (Figure 16) and of the resulting velocity fields within the boundary layer it can be seen, that behind the serpentine actuation at the mid-chord, the fluctuating kinetic energy available to the flow is moved out of the broadband spectrum and is largely put into the harmonics of the forcing frequency. Overall, the turbulent kinetic energy is large, but it is isolated into these harmonic frequencies. Closer to the trailing edge, the turbulent kinetic energy increases, but the magnitude of the turbulent kinetic energy remains smaller relative to the uncontrolled case. Furthermore, the energy stored in the peaks seems to decrease as the geometry of the actuator is straightened before increasing again for the flattest geometry tested here.

Both of these effects show interesting behavior initially. At x/c=0.1, the strength of the disturbance increases as the serpentine geometry becomes more pronounced. However, all of the TKE and PSD(St=5) drop dramatically to roughly the same levels at x/c=0.2. Over the next half chord, the growth of the disturbance frequency is almost the same for all of the actuated cases, indicating that for the forcing distribution applied, the growth rate is roughly independent of the geometry of the plasma actuator. The growth of the TKE continues slightly farther down-stream, indicating that secondary effects are also coming into play, and that additional frequencies are also of importance. Examining the power spectral

densities shown previously, the first and second (St=10.0 and 15.0, respectively) are of greater or equal importance to the flow.

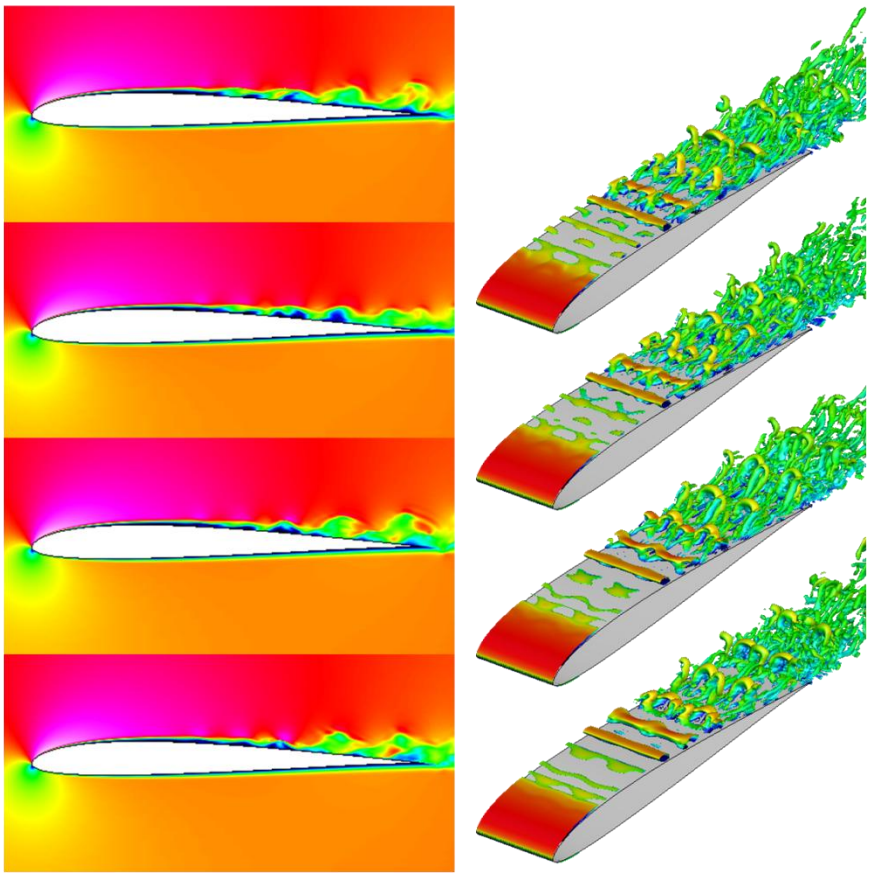

Figure 12. Instantaneous velocity magnitude (z=0.1, pinching, left) and Q-criterion (right) for pulsed serpentine plasma actuation, varying the geometry of the actuator (from top to bottom - full, three quarters, half and quarter).

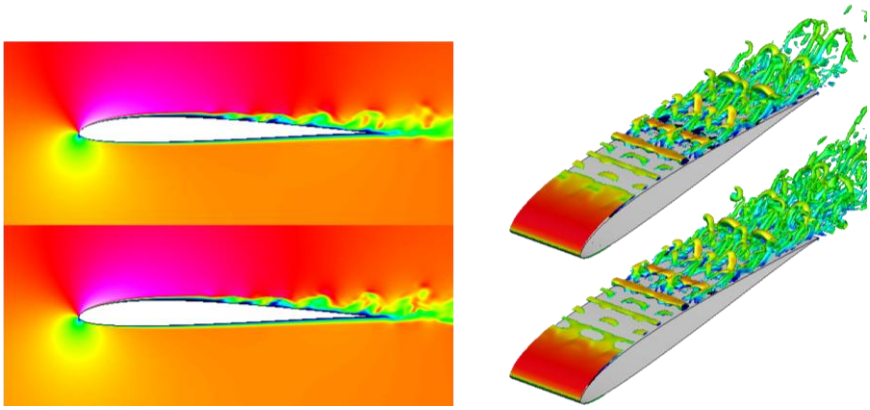

Figure 13. Comparison of phase averaged (ϕ=0) and instantaneous (bottom) velocity magnitude (left) and Q-criterion (Q=100, right) for the pulsed plasma actuation for the full geometry.

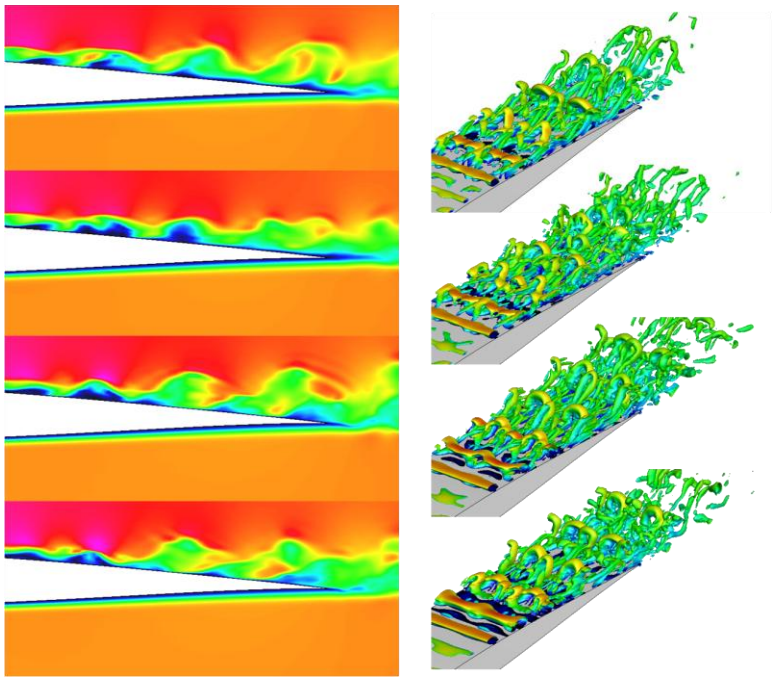

Figure 14. Phase averaged (ϕ=0) velocity magnitude (z=0.1, left) and Q-criterion (Q=100, right) near the trailing edge of the airfoil

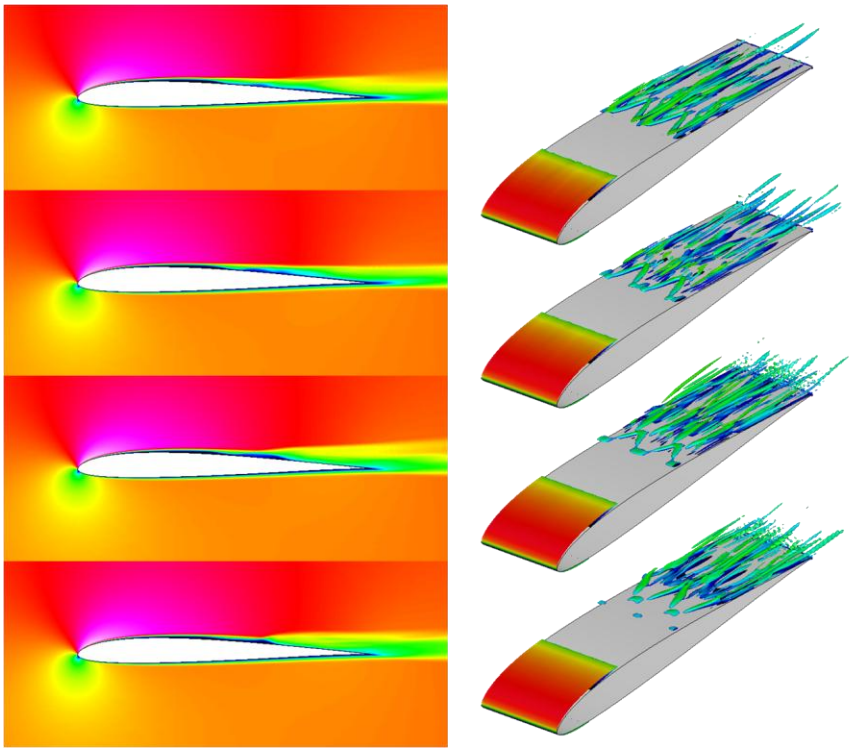

Figure 15. Time averaged velocity magnitude (z=0.1, pinching point, left) and Q-criterion (Q=100, right) from above for the various geometries (from top to bottom - full, three quarters, half and quarter).

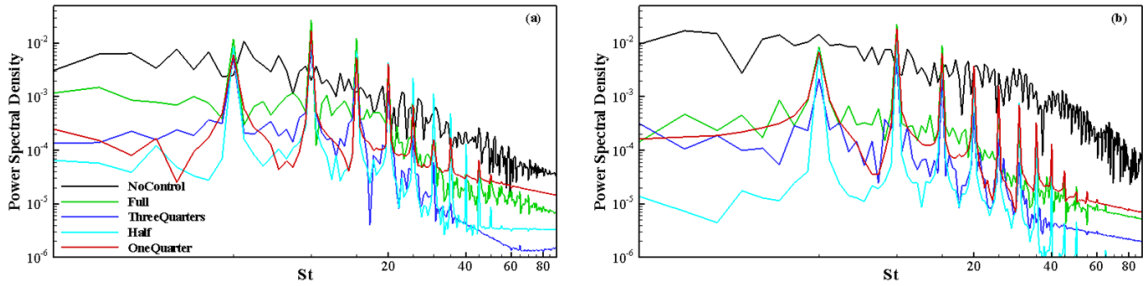

Figure 16. Power Spectral Densities for the pulsed actuation cases at (a) the midchord (x/c=0.5) and (b) near the trailing edge (x/c=0.9).

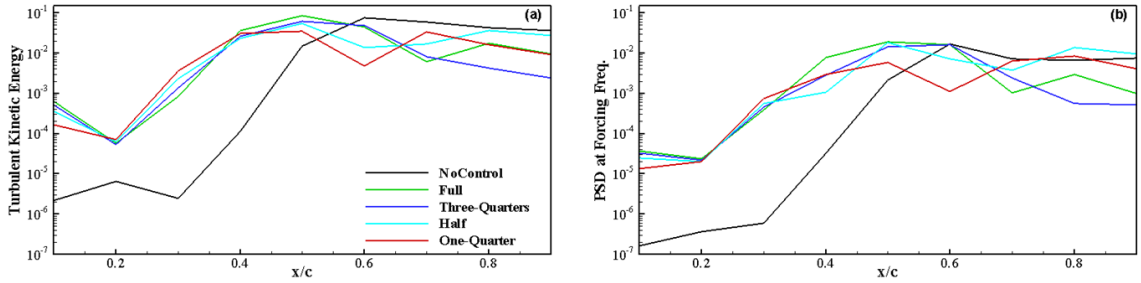

Figure 17. Growth of the turbulent kinetic energy (a) and disturbance frequency (b) along the surface of the airfoil.

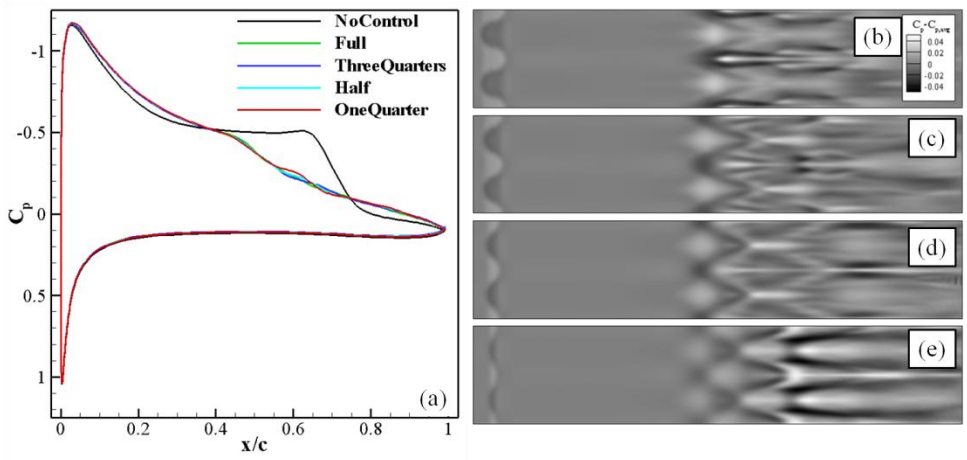

Figure 18. Surface pressure (left), C_p for the cases of pulsed serpentine actuation (a) and phase averaged local variations in the surface pressure coefficient - $C_p(x,z)$-$C_{p,avg}$ at ϕ=0. From top to bottom – Full, three quarters, half and one quarter (b-e).

D. Overall effects on lift and drag

Though the variation of the geometry shows some impact on the lift and drag, it seems that the largest driver is whether or not the plasma forcing is pulsed or not, thus indicating that the unsteady stability is the most important thing to reattaching the flow (Table 3). Pulsing the actuation seems to bring a drop in C_L and C_D, with corresponding rise in $<C_L/C_D>$ of roughly 19%, similar to the effects of reattachment for the linear actuator geometries[10-11]. Only marginal changes appear with continuously run plasma actuation, where $<C_L/C_D>$ increases only by 1.0%.

In examining the transient forces experienced by the airfoil under steady actuation, it can be seen that there is at least one important frequency present in the forces (Figure 19). This frequency is slightly lower than the St=.05 frequency seen with no actuation, suggesting that the shedding frequency of (now three

dimensional) boundary layer has changed. Furthermore, a slower level of unsteadiness seems to still exist for the continuously actuated cases. Again, this may suggest that some slow behavior exists that does not exist for the un-actuated or the pulsed actuation simulations.

The lift and drag for the cases of pulsed actuation also shows oscillatory behavior, but that behavior is consistent with the St=5 forcing frequency (Figure 20). Additionally, aside from a slight increase for the fullest serpentine geometry, the magnitude of the oscillations increases as the geometry compresses, possibly resulting from the more coherent vortical structures in the boundary layer passing over the trailing edge all at once (similar effects with spanwise vortical structures were seen previous work[10-11]). These oscillations are also smaller than those of the uncontrolled or of the continuously actuated case.

Case	$<C_L>$	$<C_D>$	$<C_M>$	$<C_L/C_D>$	C_L'	C_D'	C_M'
Baseline	0.58926	0.0246	-0.0485	23.998	0.0087	0.00091	0.0042
Full – Pulsed	0.54782	0.0193	-0.0303	28.433	0.0029	0.00028	0.0015
Full - Cont.	0.56207	0.0234	-0.0378	23.986	0.0079	0.00076	0.0032
Three Quarters – Cont.	0.56061	0.0229	-0.0372	24.508	0.0058	0.00058	0.0026
Half – Cont.	0.57124	0.0235	-0.0410	24.297	0.0064	0.00065	0.0030
One Quarter – Cont.	0.56827	0.0235	-0.0409	24.190	0.0110	0.00094	0.0043
Three Quarters – Pulsed	0.54551	0.0191	-0.0304	28.530	0.0018	0.00022	0.0010
Half – Pulsed	0.55076	0.0192	-0.0310	28.476	0.0030	0.00035	0.0020
One Quarter – Pulsed	0.55358	0.0193	-0.0318	28.678	0.0036	0.00044	0.0023

Table 3. Average (<…>) and standard deviations (') of the airfoil forces for the various cases run

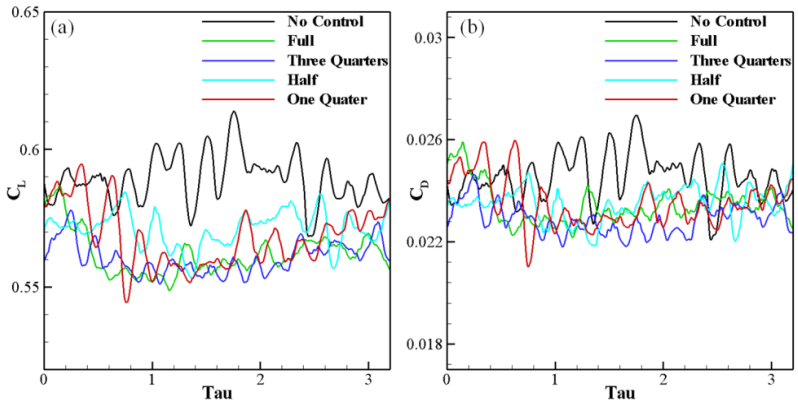

Figure 19. Time resolved C_L, (a) and C_D (b) with continuous plasma actuation.

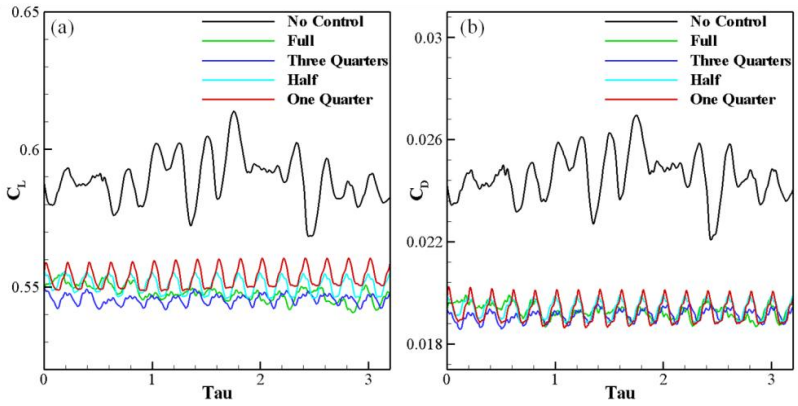

Figure 20. Time resolved C_L (a) and C_D (b) with pulsed plasma actuation.

V. Conclusions

Simulations were performed in order to better understand the effects of geometric variation using plasma actuation. While these simulations achieved the desired result of reattaching the flow and show that the fullness of the serpentine geometry impacts the flow, but that other effects are likely more important.

While serpentine geometry plasma actuation shows promise as a tool for flow control under other circumstances, it appears that for the forcing distibution tested, the geometric curvature of the electrodes does not provide additional control authority of separation mitigation. For this particular case, the stability of the separated shear layer seems to be the most important parameter, and pulsing the flow ultimately has the largest effect on reattachment.

While this device does not show significantly more or less control authority as compared to the traditional linear plasma actuator, it did show a slightly different method of control authority because it is able to apply a characteristic wave number in the spanwise direction, and influence the transition and reattachment in that manner. Future efforts could be directed towards replacing spanwise distributed roughness or some other flow control method. Further exploration of the effects of expanding into these novel geometries under canonical flow conditions may help to identify conditions where these devices may be the optimal flow control device.

Acknowledgments

This work was partially funded AFOSR grants monitored by Dr. Douglas Smith. The first author was also supported by the AFRL summer training and the University of Florida Graduate School Fellowship Award. The authors would also like to acknowledge the University of Florida High Performance Computing Center for providing computational resources for the results presented in this paper.

References

[1] Greenblatt, D. and Wygnanski, I.J. "The control of flow separation by periodic excitation," *Progress in Aerospace Sciences* Vol 36, pp 487-545, Oct 2000.

[2] Moreau, E. "Airflow control by non-thermal plasma actuators". *Journal of Physics D: Applied Physics*, Vol 40, No 1, 2007

[3] Greenblatt, D., Schule, C.Y., Romann, D., and Paschereit, C.O. "Dielectric Barrier Discharge Flow Control at Very Low Flight Reynolds Numbers," *AIAA Journal* Vol 46, No. 6, June 2008.

[4] Roth, J.R., Sherman, D. M., and Wilkinson, S. P. "Boundary Layer Flow Control with a One Atmosphere Uniform Glow Discharge Surface Plasma," AIAA Paper 98-0328, Jan 1998.

[5] Gaitonde, D.V., Visbal, M.R., and Roy, S. "Control of Transitional and Turbulent Flows Using Plasma-Based Actuators," AIAA Paper 2006-3230, June 2006.

[6] Rizzetta, D.P. and Visbal, M.R. "Plasma-Based Flow-Control Strategies for Transitional Highly Loaded Low-Pressure Turbines," *ASME Journal of Fluids Engineering*, Vol 130, No 4, April 2008.

[7] Gaitonde, D.V., Visbal, M.R., and Roy, S. "A Coupled Approach for Plasma-Based Flow Control Simulations of Wing Sections," AIAA Paper 2006-1205, Jan 2006.

[8] Gaitonde, D.V., Visbal, M.R. and Roy, S. "Control of Flow Past a Wing Section with Plasma-based Body Forces," AIAA Paper 2005-5302, June 2005.

[9] Gaitonde, D.V., Visbal, M. R., and Roy, S. "Three-dimensional Plasma-Based Stall Control Simulations with Coupled First-Principals Approaches," ASME Paper FEDSM2006-98553, July 2006.

[10] Rizzetta, D.P. and Visbal, M.R. "Numerical Investigation of Plasma-Based Control for Low-Reynolds Number Airfoil Flows," AIAA paper 2010-4255.

[11] Riherd, P.M., Roy, S, Rizzetta, D. and Visbal, M.R. "Study of Transient and Unsteady Effects of Plasma Actuation in Transitional Flow over an SD7003 Airfoil," AIAA Paper 2011-1075.

[12] Wang, C.C. and Roy, S. "Electrodynamic Enhancement of Film Cooling Of Turbine Blades," *Journal of Applied Physics* 104, Oct 2008.

[13] Roy, S. and Wang, C.C., "Bulk flow modification with horseshoe and serpentine plasma actuators," *Journal of Physics D: Applied Physics*, Vol 42. 2009.

[14] Wang, C.C., Durscher, R. and Roy, S., "Three-dimensional effects of curved plasma actuators in quiescent air, *Journal of Applied Physics*, Vol 109, 2011.

[15] Schatzman, D.M. and Thomas, F.O. "Turbulent Boundary Layer Separation Control with Plasma Actuators," AIAA Paper 2008-4199, June 2008.

[16] Santhanakrishnan, A. and Jacob, J., "Flow control with plasma synthetic jet actuators," *Journal of Physics D: Applied Physics*, Vol 40, 2007.
[17] Durscher, R. and Roy, S., "Induced Flow from Serpentine Actuators Acting in Quiescent Air," AIAA Paper 2011-957, Jan 2011.
[18] Rizzetta, D.P., Visbal, M.R., and Morgan, P.E. "A High-Order Compact Finite-Difference Scheme for Large-Eddy Simulation of Active Flow Control" AIAA Paper 2008-526, Jan 2008.
[19] Visbal, M. R. and Gaitonde, D. V., "High-Order-Accurate Methods for Complex Unsteady Subsonic Flows," *AIAA Journal*, Vol 37, No.10, Oct 1999, pp 1231-1239.
[20] Beam, R.M. and Warming, R.F. "An Implicit Factored Scheme for the Compressible Navier-Stokes Equations," *AIAA Journal* Vol 16, No 4, April 1978.
[21] Lele, C. A., "Compact Fine Difference Schemes with Spectral-Like Resolution," *Journal of Computational Physics*, Vol 102, No. 1, 1992, pp. 16-42.
[22] Singh, K.P. and Roy, S. "Force approximation for a plasma actuator operating in atmospheric air," *Journal of Applied Physics*, Vol 103, No. 1, 2008.
[23] Galbraith, M. C. and Visbal, M.R. "Implicit Large Eddy Simulation of Low Reynolds Number Flow Past the SD7003 Airfoil," AIAA paper 2008-225, Jan. 2008.
[24] Galbraith, M.C. and Visbal, M.R. "Implicit Large Eddy Simulation of Low-Reynolds-Number Transitional Flow Past the SD7003 Airfoil," AIAA paper 2010-4737. July, 2010.
[25] Ol, M.V., McAuliffe, B.R., Hanff, E.S., Scholz, U, and Kahler, C. "Comparison of Laminar Separation Bubble Measurements on a Low Reynolds Number Airfoil in Three Facilities" AIAA Paper 2005-5149, June 2005.
[26] Hunt, J. C. R. , Wray, A. A. and Moin, P. "Eddies, stream, and convergence zones in turbulent flows," *Report* — CTR-S88, Center For Turbulence Research, 1998.
[27] Acarlar, M.S., and Smith, C.R., "A study of hairpin vortices in a laminar boundary layer. Part 1. Hairpin vortices generated by a hemispherical protuberance," *Journal of Fluid Mechanics*, Vol 175, pp 1-41. 1987.
[28] Acarlar, M.S., and Smith, "A study of hairping vortices in a laminar boundary layer. Part 2. Hairpin vortices generated by fluid injection" *Journal of Fluid Mechanics*, Vol 175, pp 43-83. 1987.
[29] Zhou, J., Adrian, R.J., Balchandar, S. and Kendally, T.M., "Mechanisms for generating coherent packets of hairpin vortices in channel flow," *Journal of Fluid Mechanics*, Vol 387, pp 353-396.